Chinese Journal of Polymer Science Vol. 31, No. 1, (2013), 12–20

Chinese Journal of Polymer Science

TWO-LAYER MODEL DESCRIPTION OF POLYMER THIN FILM DYNAMICS*

Dong-dong Peng[a], Ran-xing Nancy Li[a], Chi-hang Lam[b] and Ophelia K.C. Tsui[a**]
[a] *Department of Physics, Boston University, Boston, MA 02215, U.S.A.*
[b] *Department of Applied Physics, Hong Kong Polytechnic University, Hong Kong, China*

Abstract Experiments in the past two decades have shown that the glass transition temperature of polymer films can become noticeably different from that of the bulk when the film thickness is decreased below *ca.* 100 nm. It is broadly believed that these observations are caused by a nanometer interfacial layer with dynamics faster or slower than that of the bulk. In this paper, we examine how this idea may be realized by using a two-layer model assuming a hydrodynamic coupling between the interfacial layer and the remaining, bulk-like layer in the film. Illustrative examples will be given showing how the two-layer model is applied to the viscosity measurements of polystyrene and polymethylmethacrylate films supported by silicon oxide, where divergent thickness dependences are observed.

Keywords: Polymer films; Glass transition; Viscosity.

INTRODUCTION

It has been broadly observed that the glass transition temperature, T_g, of polymer films can become visibly different from the bulk one when the film thickness, h, is decreased to less than *ca.* 100 nm[1–20]. Both T_g reduction[1–17] and enhancement[1, 18–21] have been observed. Most believe that T_g reduction is caused by a mobile layer located at the free surface[1–8, 11–17, 22–29] while T_g enhancement is caused by a dynamically impeded layer located at the substrate surface of the films[18–20, 30–33]. Experiments showed that the anomalous dynamics at the interfaces persisted for several nanometers only[15, 29, 33], raising questions concerning how they may produce long-range effects in the films up to 100 nm, where anomalous T_g began to occur. Recently, we showed that a two-layer model consisting of a surface mobile layer at the top of the film, hydrodynamically coupled to the bottom, bulk-like layer could explain the thickness dependence found of the viscosity, $\eta(h)$, of polystyrene (PS) films with molecular weights of 2.4[34] and 212 kg/mol[29, 35].

In this study, we expand the two-layer model description to cases where the interfacial layer can be slower than the bulk, and/or located at the substrate interface. For illustration, we compare the model predictions to the viscosity measurements of PS films with molecular weight, M_w = 13.2 and 60.5 kg/mol and atatic poly(methyl methacrylate) (PMMA) films with M_w = 2.7 kg/mol, both supported by silicon oxide, where divergent thickness dependences are observed. We find that the data of both systems can be fitted well to the two-layer model, provided a surface mobile layer is assumed in the former and a slow substrate layer in the latter.

* The work was financially supported by the National Science Foundation through the projects DMR-0908651 and DMR-1004648, and HK PolyU through the grant G-U857.
** Corresponding author: Ophelia K. C. Tsui, E-mail: okctsui@bu.edu
Invited lecture presented at the International Symposium on Polymer Physics, 2012, Chengdu, China
Received July 11, 2012; Revised August 24, 2012; Accepted August 28, 2012
doi: 10.1007/s10118-013-1207-x

EXPERIMENTAL

Sample Preparation

Polystyrene with M_w of 13 and 61 kg/mol (denoted 13 K and 61 K PS below) and polydispersity of 1.06 and 1.3, respectively, were purchased from Scientific Polymer Products (Ontario, NY). Poly(methyl methacrylate) with a M_w of 2.7 kg/mol (denoted 2.7K PMMA below) and polydispersity of 1.09 was purchased from Polymer Source (Dorval, Quebec). According to the manufacturer, it has a tacticity (%) of 7:24:69 (isotatic:heterotatic: syndiotatic). Silicon (100) wafers covered with a 102 nm thick oxide and cut into 1.5 cm × 1.5 cm slides were used as the substrate. Prior to use, the slides were cleaned in a piranha solution as described before[15, 34]. Thin films of the polymers, with thickness, h, varied between 3 nm and 86 nm, were spin-coated onto the cleaned substrates from toluene solutions of the polymers and measured without pre-annealing. The film thickness was controlled by varying the concentration of the solution, and measured by ellipsometry. The viscosity of the films was determined by monitoring the evolution of the surface topography during the initial stage of dewetting[36] when the surface roughness was much less than the film thickness and well before any holes formed. We used tapping-mode atomic force microscopy (AFM) to measure the surface topography. To facilitate the data analysis (to be discussed below), we convert the topographic data to power spectral density (PSD) by multiplying them with a Welch function, Fourier-transforming the product then radial averaging the result[37, 38].

Method to Measure the Viscosity of the Films

Previously we showed that as-cast spin-coated polymer films were smoother than equilibrium[35, 38], so roughened upon heating at an elevated temperature[39]. The roughening process of the films, whether unentangled[37, 38] or entangled[38], can be described by:

$$A_q^2(t) = A_q^2(0) + \left[\frac{k_B T}{G''(h) + \gamma q^2} - A_q^2(0)\right]\left(1 - \exp(2\Gamma_q t)\right) \tag{1}$$

where $A^2_q(t)$ is the PSD, q is the wavevector, k_B is the Boltzmann constant; h, T, $G(h)$ and $\gamma$is, respectively, the average film thickness, annealing temperature in Kelvin, van der Waals potential[35, 38], and surface tension of the film. From Eq. (1), it is apparent that the roughening dynamics is governed by Γ_q, *i.e.*, the dynamic rate of the surface capillary mode with wavevector q[35, 38]. For unentangled polymer films[39],

$$\Gamma_q = -Mq^2[\gamma q^2 + G''(h)] \tag{2}$$

where M is the flow mobility and given by[40]:

$$M = \frac{h^3}{3\eta} \ . \tag{3}$$

The parameter η is the effective viscosity of the film, namely the viscosity of the film if it had been uniform and did not possess any spatial dynamic heterogeneity.

As for entangled polymer films, if they are initially in the rubbery state with elastic modulus μ_0, but crossover to the terminal flow regime with viscosity η after annealing for time, t, greater than the relaxation time, $\tau \equiv \eta/\mu_0$, Γ_q is given by[15]:

$$\Gamma_q = -Mq^2\left[\left(\gamma q^2 + G''(h)\right)^{-1} + \left(\frac{3\mu_0}{h^3 q^2}\right)^{-1}\right]^{-1} \ . \tag{4}$$

In comparing Eqs. (2) and (4), it is evident that addition of a transient shear modulus μ_0 to the films (for times $t \le \tau$) uniformly lengthens the relaxation time of all the capillary modes by $[Mq^2(3\mu_0{}^2/h^3q^2)]^{-1}$ (which one can show is just τ), resulting in a lower limit of $1/\Gamma_q > \tau$ for the characteristic time of the modes. Consequently, the capillary modes and hence the PSDs do not evolve noticeably until the annealing time goes beyond τ[15]. This

prediction is clearly seen in the data of Fig. 1, representative of the PSD's obtained in this experiment. The solid lines represent the best fit of the data to Eqs. (1) and (4) with μ_0 and η treated as fitting parameters, while T and h are given the experimental values, and k_B and $G''(h)$[15] the literature values. The surface tension, γ, is deduced by fitting the high-q region of the data to $k_BT/\gamma q^2$ (see the heavy dashed line in Fig. 1), where we usually obtain values between 0.03 Jm^{-2} and 0.04 Jm^{-2}, consistent with the values found in literature[41].

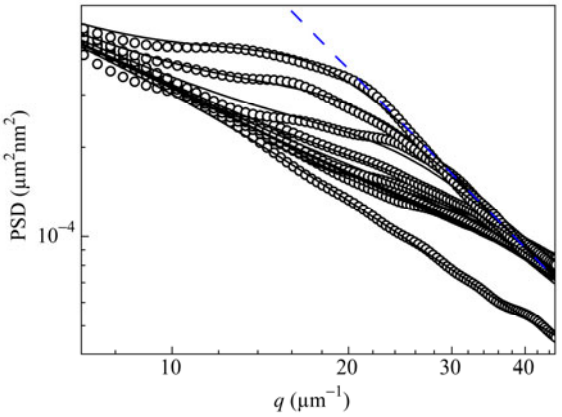

Fig. 1 Power spectral density (PSD) of a 13 nm thick PS film (M_w = 212 kg/mol) coated on silicon oxide upon annealing at T = 120°C (symbols)
The measurement times of the PSD are (from bottom to top): 0, 960, 3840, 7680, 30720, 61440, 184320, 368640 and 737280 s. The solid lines are the best fit to Eqs. (1) and (4). The dash line is the best fit of the high-q region of the data to $k_BT/\gamma q^2$, resulting in a fitted value of 0.037 J/m^2 for γ. Adapted with permission from Ref. [38] (Copyright 2012 American Chemical Society)

THEORETICAL BACKGROUND

In this section, we briefly describe the two-layer model previously developed to explain the viscosity measurements of PS supported films[15, 29]. In this model, the films are assumed to be open-top channels with infinitely large lateral extent and contain a two-layer fluid with total depth, h. The thickness and viscosity of the top (bottom) layer is denoted by h_t ($h_b \equiv h - h_t$) and η_t (η_b), respectively (see Fig. 2). We solve the Navier-Stokes equation for the steady flow pattern in such a channel due to an applied uniform pressure gradient, ∇P, parallel to the channel. By assuming the no-slip boundary condition at the bottom surface, zero interfacial tension between the two layers, and zero stress at the free surface, the fluid velocity profile in the fluid, $v(z)$, where z is the distance from the channel bottom, is found to be[15, 38]:

$$v(z) = \frac{-\nabla P}{2\eta_b}\left[z^2 - 2(h_b + h_t)z\right] \qquad (z < h_b)$$

and

$$v(z) = \frac{-\nabla P}{2\eta_t}\left[(z - h_b)^2 - 2h_t(z - h_b) - \frac{\eta_t}{\eta_b}h_b(2h_b + h_t)\right] \qquad (z > h_b)\,. \tag{5}$$

By using this result, we calculate the total mobility of the film[41]:

$$M = \frac{h_b^3}{3\eta_b} + \frac{h_t^3}{3\eta_t} + \frac{h_t h_b (h_b + h_t)}{\eta_b}\,. \tag{6}$$

The first two terms are the mobilities of the individual layers should the other layer be absent. The third is a hydrodynamic coupling term. Combining Eqs. (3) and (6), we derive the effective viscosity of the two-layer

film:

$$\eta \equiv \frac{h^3}{3M} = \left[\left(\frac{h_t}{h} \right)^3 \frac{1}{\eta_t} + \left(\frac{h_b^3 + 3h_t h_b h}{h^3} \right) \frac{1}{\eta_b} \right]^{-1} . \quad (7)$$

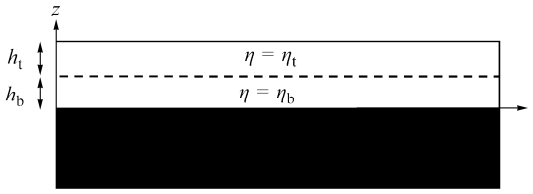

Fig. 2 Schematic showing the parameters in the two-layer model

RESULTS AND DISCUSSIONS

Experimental Results

We first discuss the experimental results of the PS and PMMA films. The solid symbols in Fig. 3(a) display the effective viscosity, η, of the 13K and 61K PS films measured at 120°C, plotted versus the film thickness, h. For comparison, the corresponding data of the 2.4K PS films obtained previously at 75°C[15] are also shown (open circles). As seen, the data of all the films exhibit similar dependences on h. Specifically at large h, they asymptotically approach a constant consistent with the published bulk viscosity, η_{bulk}, of the respective polymer within a factor of 2.5. But for small h, they asymptotically approach a $\sim h^3$ dependence. The solid lines display the best fits of the 13K and 61K data to the Two-layer model (Eq. (7)), with values of the fitted parameters given in Table 1. The dashed line displays the two-layer model fit to the 2.4K data reported in Ref. [15]. Figure 3(b) shows the same data displayed in Fig. 3(a), but normalized by the fitted values of η_{bulk}, namely 6.3, 0.32 and 50 MPas for the 2.4K, 13K and 61K films, respectively. In this plot, it is apparent that the thickness, where the crossover between the large and small h asymptotes takes place, depends on the value of η(3 nm)/η_{bulk} only. Specifically, the smaller this ratio is, the bigger the crossover thickness. We provide an explanation to this observation below.

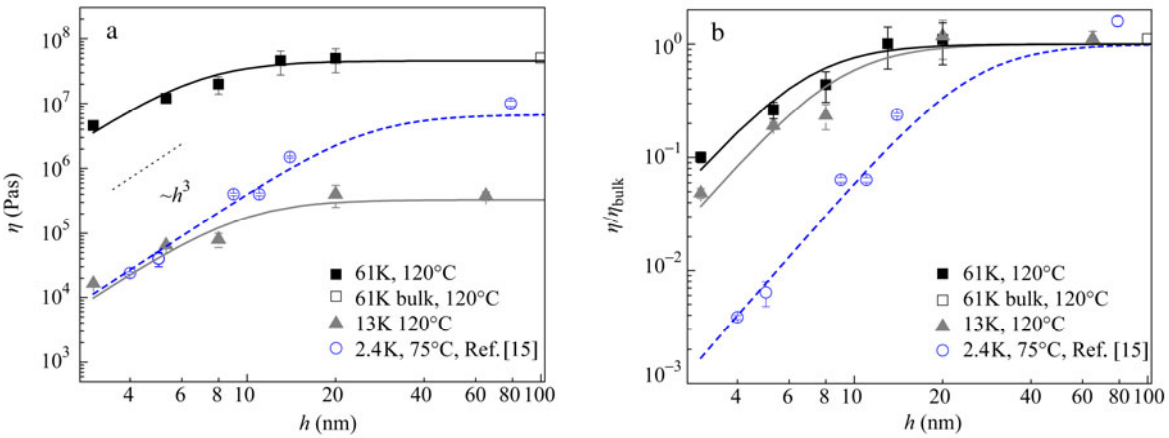

Fig. 3 (a) Effective viscosity of the PS films (solid symbols) measured at 120°C plotted versus film thickness (The open square represents the published viscosity of 61K bulk PS[42]. The solid lines represent the best fits of the 61K and 13K data to the two-layer model (Eq. (7)) using η_t and η_{bulk} as the fitting parameters while h_t is set equal to 3 nm. The open circles and dashed line are the data and two-layer model line of 2.4K PS films extracted from Ref. [15]. The dotted line illustrates the h^3 power-law dependence.), (b) the same data shown in (a) but normalized by the respective fitted value of η_{bulk}

Table 1. Summary of the fitted parameters of the two-layer model obtained in this study

Sample	h_t (nm)	η_t (Pas)	h_b (nm)	η_b (Pas)	η^*/η_{bulk}
61K PS (120°C)	$h^* = 3$[a, d]	η^* (see last column)	$\equiv (h - h^*)$[b, d]	$\eta_{bulk} = 10^{(7.7 \pm 0.1)}$	0.08 ± 0.03
13K PS (120°C)	$h^* = 3$[a, d]	η^* (see last column)	$\equiv (h - h^*)$[b, d]	$\eta_{bulk} = 10^{(5.5 \pm 0.2)}$	0.04 ± 0.03
2.7K PMMA (140°C)	$\equiv (h - h^*)$[b, d]	$\eta_{bulk} = 2000$[c, d]	$h^* = 1.5 \pm 0.25$	η^* (see last column)	18 ± 6

[a]This is the mobile layer thickness. Being covariant with η_t, we fix its value to 3 nm (see discussion in the text);
[b]This is the bulklike layer thickness, $h - h^*$, where h is the total thickness of the film;
[c]This is the measured viscosity at $h = 86$ nm and the same as the published bulk viscosity[41];
[d]The shading indicates that the parameter was not fitted.

The open triangles in Fig. 4 show the normalized viscosity, η/η_{bulk} of the 2.7K PMMA films measured at 140°C, where $\eta_{bulk} = 2000$ Pas is the viscosity of the 86 nm film and also the bulk polymer[41]. For thick enough films ($h >$ *ca.* 40 nm), $\eta/\eta_{bulk} \approx 1$ as expected. For thinner films ($h <$ *ca.* 40 nm), η/η_{bulk} increases continuously with decreasing h, contrary to the $\eta(h)$ dependence found of the PS films. Nevertheless, we are still able to obtain good fits to the data by using the two-layer model (solid line in Fig. 4), provided the interfacial layer is assumed to be more viscous than the bulk and located at the substrate surface. The fitted parameters are displayed in Table 1.

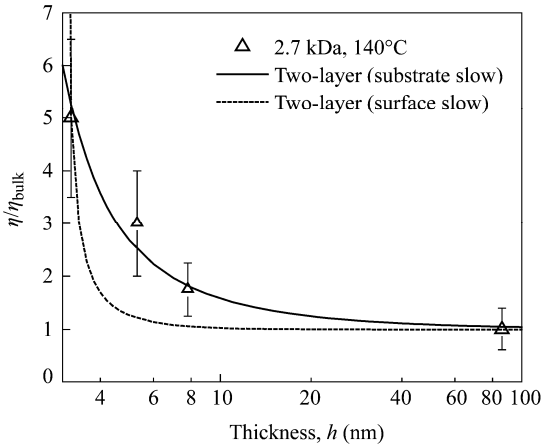

Fig. 4 Measured effective viscosity of the PMMA films at 140°C, η, normalized by the literature value of η_{bulk} (= 2000 Pas), plotted versus film thickness, h
The solid line represents the best fit to the two-layer model (Eq. (7)) when η_b and h_b are co-varied and η_{bulk} set equal to 1. This corresponds to the substrate slow case. The dashed line shows the best fit to the two-layer model in the surface slow case (Eq. (8)).

The above results show that the two-layer model is capable of describing the divergent $\eta(h)$ behaviors found in experiment. On the other hand, given the simplicity of the $\eta(h)$ dependences observed (Figs. 3 and 4), it is not obvious if the four-parametered two-layer model is able to accurately determine the dynamic heterogeneity of the films without obscures from possible alternative parameter sets that may also fit the experimental data. Below, we elaborate the different possible cases of the two-layer model and discuss how they may be differentiated among each other, and be used to reliably discern the dynamic heterogeneity in the films.

Two-layer Model Description for the Experiment

A mundane but important property of the experimental $\eta(h)$ dependence is that it always asymptotically approaches the bulk viscosity at large h. This suggests that one of the layers must be bulklike and has a thickness approaching h when h is infinitely large. Correspondingly, we designate the viscosity and thickness of this layer

to be η_{bulk}, and $h - h^*$, respectively, where h^* is the thickness of the other, non-bulklike layer. Given these, there are four possible cases according to whether the top or bottom layer is non-bulklike and how the viscosity of the non-bulklike layer (denoted by η^* below) compares to η_{bulk}. Below we discuss each of these cases.

Case 1: Surface mobile layer ($h_t \equiv h^*$ and $\eta_t \ (\equiv \eta^*) < \eta_b \ (\equiv \eta_{bulk})$)

As discussed above, this case agrees with the data of the PS films. A representative velocity profile, $v(z)$, is shown in Fig. 5(a). By applying the specifics of this case, namely, $h_t = h^*$, $\eta_t = \eta^*$ and $\eta_b = \eta_{bulk}$ to Eq. (7), we obtain the following expression for the normalized viscosity:

$$\begin{aligned}\frac{\eta}{\eta_{bulk}} &= \left[\left(\frac{\eta_{bulk}}{\eta^*}\right)\left(\frac{h^*}{h}\right)^3 + \left(\frac{(h-h^*)^3 + 3h^*(h-h^*)h}{h^3}\right)\right]^{-1} \\ &= \left[1 + \left(\frac{\eta_{bulk}}{\eta^*} - 1\right)\left(\frac{h^*}{h}\right)^3\right]^{-1}.\end{aligned} \tag{8}$$

From Eq. (8), one can see that there are two thickness regimes.

(a) Thin film regime ($h << (\eta_{bulk}/\eta^* - 1)^{1/3} h^*$)

In this regime, Eq. (8) gives:

$$\frac{\eta}{\eta_{bulk}} \cong \left(\frac{\eta_{bulk}}{\eta^*} - 1\right)^{-1}\left(\frac{h}{h^*}\right)^3. \tag{9}$$

It predicts that the effective viscosity converges to a $\sim h^3$ dependence when h approaches zero.

(b) Thick film regime ($h >> (\eta_{bulk}/\eta^* - 1)^{1/3} h^*$)

In this case, Eq. (8) predicts that $\eta/\eta_{bulk} \to 1$. In other words, the effective viscosity approaches the bulk viscosity when h is infinitely large.

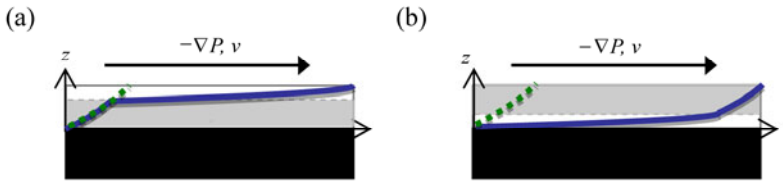

Fig. 5 Typical solutions to the velocity profile, $v(z)$, of the fluid in a two-layer film due to a horizontal pressure gradient, ∇P, according to Eq. (4): (a) a case where the top layer is thin and more mobile than the bottom layer and (b) a case where the two layers in (a) are exchanged
The $v(z)$ profile is shown by the thick solid line in both drawings. For comparison, the corresponding velocity profile for a uniform film with the same viscosity as the slower layer is shown by the thick dotted line

From the data shown in Fig. (3), it is apparent that both asymptotic behaviors predicted above are observed in experiment. In addition, one can see that all the data points at h = 3 nm lie in the thin film regime. So, we apply Eq. (9) to h = 3 nm and deduce that $\eta(3\text{ nm}) = \eta_{bulk}(\eta_{bulk}/\eta^* - 1)^{-1}(3\text{ nm}/h^*)^3$. This result suggests that the crossover thickness can be re-expressed as $[\eta_{bulk}/\eta(3\text{ nm})]^{1/3}(3\text{ nm})$, which clearly depends on the value of $\eta(3\text{ nm})/\eta_{bulk}$ only and so provides an explanation to the above observation. We also notice that the experimentally found values of η^*/η_{bulk} in the surface mobile case is often << 1 (see the values of PS films in Table 1). With this, Eq. (9) gives $\eta/\eta_{bulk} \approx (1 + M^*/M_{bulk})^{-1}$ or $M \approx M^* + M_{bulk}$, where $M^* \equiv h^{*3}/3\eta^*$ and $M_{bulk} \equiv h^3/3\eta_{bulk}$ is the mobility of the surface mobile layer and a uniform film with thickness h and viscosity η_{bulk}, respectively. In fact, this approximation has been used before[15, 29] and found to produce excellent fits to the

experimental data. Another noteworthy observation is that η^* and h^* are not independent parameters in Eq. (8). Specifically, any combinations of the two giving the same $(\eta_{bulk}/\eta^* - 1)^{1/3}h^*$ will give the same $\eta(h)/\eta_{bulk}$ dependence. As a result, it is not possible to determine the values of η^* and h^* separately by fitting the experimental data to Eq. (8) (namely, the surface mobile case). Meanwhile, we observe that the data of Fig. 3 are still varying with h at h = 3 nm. This means that the surface mobile layer thickness, h^*, must be ≤ 3 nm, for otherwise the 3 nm films constitute a uniform single layer and the data should exhibit a plateau at h = 3 nm. In fitting the data, we have assumed h^* = 3 nm, *i.e.*, the smallest thickness used in this study, with the understanding that the fitted value of η^* hence obtained (Table 1) is slaved to the value of h^* assumed. But as pointed out above, Eq. (8) is approximately equivalent to the expression, $M = M^* + h^3/3\eta_{bulk}$, where M^* is evidently an independent parameter. If one fits the approximate expression to the data, one would find that the (unique) fitted value of M^* is related to the value of η^* obtained above by $M^* = (3\text{ nm})^3/3\eta^*$ and does not depend on the choice of h^* used.

Case 2: Substrate mobile layer (h_b is $\equiv h^*$ and η_b ($\equiv \eta^*$) < η_t ($\equiv \eta_{bulk}$))

The fact that the measured η/η_{bulk} of PS films is always ≤ 1 (see Fig. 3) means that a mobile layer is involved. But a priori, it is not obvious where one should assume its location to be. In Case 1, we considered the situation where the mobile layer is located at the top. Here, we consider the situation where it is located at the bottom. A representative velocity profile, $v(z)$, of this case is shown in Fig. 5(b). By applying the case specifics, namely $h_b = h^*$, $\eta_b = \eta^*$ and $\eta_t = \eta_{bulk}$ to Eq. (7), we obtain:

$$\frac{\eta}{\eta_{bulk}} = \left[\left(\frac{h-h^*}{h}\right)^3 + \left(\frac{\eta_{bulk}}{\eta^*}\right)\left(\frac{h^{*3}+3h^*(h-h^*)h}{h^3}\right)\right]^{-1} = \left\{1+\left[\frac{\eta_{bulk}}{\eta^*}-1\right]\cdot\left[1-\left(\frac{h-h^*}{h}\right)^3\right]\right\}^{-1}. \tag{10}$$

Equation (10) shows that η/η_{bulk} increases slowly with increasing h and asymptotically approaches 1 when h/h^* becomes infinitely large. We deduce that for η/η_{bulk} to reach 90%, h/h^* needs to be > $[1 - (1 - 0.1/\beta)^{1/3}]^{-1}$, where $\beta \equiv \eta_{bulk}/\eta^* - 1$. If $\eta_{bulk}/\eta^* = 5$, say, this gives $h/h^* \approx 120$. In contrast, the corresponding value of h/h^* in Case 1 is only 3.4. Figure 6(a) shows plots of the calculated $\eta(h)/\eta_{bulk}$ discussed in this example. The large difference seen in the thicknesses required to recover the bulk behavior may be perceived from the notably different velocity profiles of the two cases (Fig. 5). For Case 1, the velocity profile deviates from that of a uniform, bulklike film only for $z > h - h^*$ (thick dashed line in Fig. 5a). But for Case 2, the deviation begins from z = 0 and accumulates over the whole film (thick dashed line in Fig. 5b), giving rise to a significantly larger alteration to the total horizontal fluid current (= integration of $v(z)$ across z) and hence the total mobility, M. The visibly different rates of recovery to the bulk behavior suggest that one should be able to unambiguously distinguish if the mobile layer is located at the film top or bottom from the data.

Case 3: Surface slow layer ($h_t \equiv h^*$ and η_t ($\equiv \eta^*$) > η_b ($\equiv \eta_{bulk}$))

The condition is geometrically the same as that in Case 1, so Eq. (8) is applicable. The dashed line in Fig. 6(b) is a plot of the $\eta(h)/\eta_{bulk}$ calculated by using Eq. (8) and η^*/η_{bulk} = 5. As one can see, $\eta(h)/\eta_{bulk}$ falls quickly from η^*/η_{bulk} at h^* to the asymptotic value of 1 as h increases. The rapid settlement to the bulk behavior is due to the small perturbation the slow layer has on the velocity profile relative to that found in a uniform bulklike film.

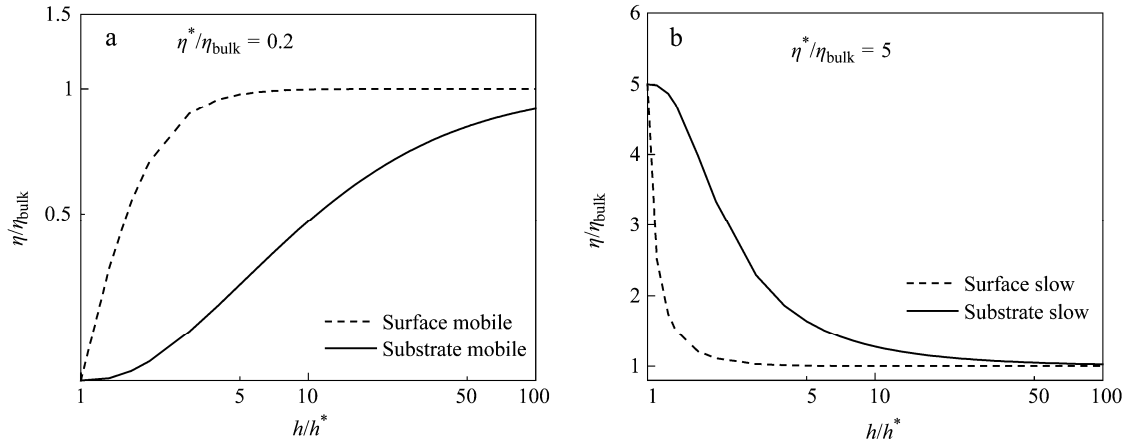

Fig. 6 (a) Calculated effective viscosity normalized by bulk viscosity calculated by using the two-layer model for Cases 1 (dashed line) and 2 (solid line) containing a mobile layer with viscosity 1/5 times the bulk viscosity and (b) corresponding plots for Cases 3 and 4 where a slow layer with viscosity 5 times the bulk viscosity is present at the top (dashed line) and bottom interface (solid line), respectively, of the film

Case 4: Substrate slow layer ($h_b \equiv h^*$ and η_b ($\equiv \eta^*$) > η_t ($\equiv \eta_{bulk}$))

The geometry is the same as that in Case 2, so Eq. (10) can be used. The solid line in Fig. 6(b) shows a plot of the $\eta(h)/\eta_{bulk}$ calculated by using Eq. (10) and η^*/η_{bulk} = 5. It also goes from the value at $h = h^*$ to 1 as the film thickness increases. But compared to Case 3, the recovery is notably slower. Again, the discrepancy can be understood by considering the perturbation to the velocity profile due to the presence of the slow layer. Alternatively, one may consider Eq. (10) in the $h >> h^*$ limit. In this limit, Eq. (10) gives $\eta/\eta_{bulk} \approx [1 + (\eta_{bulk}/\eta^* - 1)(h^*/h)]^{-1}$, which evidently approaches 1 more slowly than Eq. (8) does. So unless h^* is much smaller than the smallest film thickness studied in experiment, one should be able to distinguish the location of the slow layer from experiment, as demonstrated by the best fits of the slow substrate (solid line) and slow surface (dashed line) cases to the PMMA data in Fig. 4.

CONCLUSIONS

In conclusion, we have discussed how the local dynamics within several nanometers from an interface may affect the global dynamics of a film by using the two-layer model. Four possible cases, involving a non-bulklike layer situated at the top and bottom interface, respectively, of a film have been discussed. We found that only the case involving a mobile layer residing at the top is able to fit the viscosity measurements of PS films supported by silicon oxide while only the one involving a slow layer residing at the bottom can fit the data of PMMA films supported by silicon oxide. A detailed comparison between the predictions of the different cases shows that the respective thickness dependences of the thin film viscosity are sufficiently distinct that one should be able to discern the properties of the non-bulklike layer by fitting the experimental data to the model.

ACKNOWLEDGEMENTS We thank Prof. Z. Yang for assistance with the experiment.

REFERENCES

1 Keddie, J.L., Jones, R.A.L. and Cory, R.A., Eur. Phys. Lett., 1994, 27: 59
2 Forrest, J.A., Dalnoki-Veress, K., Stevens, J.R. and Dutcher, J.R., Phys. Rev. Lett., 1996, 77: 2002
3 Dalnoki-Veress, K., Forrest, J.A., Murray, C., Gigault, C. and Dutcher, J.R., Phys. Rev. E, 2001, 62: 5187

4 Kim, J.H., Jang, J. and Zin, W.C., Langmuir, 2000, 16: 4064
5 Roth, C.B. and Dutcher, J.R., Eur. Phys. J. E, 2003, 12: 103
6 Herminghaus, S., Jacobs, K. and Seemann, R., Eur. Phys. J. E, 2001, 5: 531
7 Herminghaus, S., Eur., Phys. J. E, 2002, 8: 237
8 Ellison, C.J. and Torkelson, M., Nature Mat., 2003, 2: 695
9 Ellison, C.J., Mundra, M.K. and Torkelson, J.M., Macromolecules, 2005, 38: 1767
10 Pye, J.E. and Roth, C.B., Phys. Rev. Lett., 2011, 107: 235701
11 Tsui, O.K.C., Russell, T.P. and Hawker, C.J., Macromolecules, 2001, 34: 5535
12 Tsui, O.K.C. and Zhang, H.F., Macromolecules, 2001, 34: 9139
13 Xie, F., Zhang, H.F., Lee, F.K., Du, B., Tsui, O.K.C., Yokoe, Y., Tanaka, K., Takahara, A. and Kajiyama, T., Macromolecules, 2002, 35: 1491
14 Tsui, O.K.C., "Polymer thin films", World Scientific, Singapore, 2008, p. 267
15 Yang, Z., Fujii, Y., Lee, F.K., Lam, C.H. and Tsui, O.K.C., Science, 2010, 328: 1676
16 Yang, Z., Peng, D., Clough, A., Lam, C.H. and Tsui, O.K.C., Eur. Phys. J. Special Topics, 2010, 189: 155
17 Clough, A., Peng, D., Yang, Z. and Tsui, O.K.C., Macromolecules, 2011, 44: 1649
18 Wallace, W.E., van Zanten, J.H. and Wu, W.L., Phys. Rev. E, 1995, 52: R3329
19 van Zanten, J.H., Wallace, W.E. and Wu, W.L., Phys. Rev. E, 1996, 53: R2053
20 Grohens, Y., Brogly, M., Labbe, C., Marie-Odile, D. and Schultz, J., Langmuir, 1998, 14: 2929
21 Sharp, J.S. and Forrest, J.A., Phys. Rev. E, 2003, 67: 031805
22 Kajiyama, T., Tanaka, K. and Takahara, A., Macromolecules, 1995, 28: 3482
23 Tanaka, K., Taura, A., Ge, S.R., Takahara, A. and Kajiyama, T., Macromolecules, 1996, 29: 3040
24 Kajiyama, T., Tanaka, K. and Takahara, A., Macromolecules, 1997, 30: 280
25 Baschnagel, J. and Binder, K., Macromolecules, 1995, 28: 6808
26 Wallace, W.E., Fischer, D.A., Efimenko, K., Wu, W.L. and Genzer, J., Macromolecules, 2001, 34: 5081
27 Fakhraai, Z. and Forrest, J.A., Science, 2008, 319: 600
28 Paeng, K., Swallen, S.F. and Ediger, M.D., J. Am. Chem. Soc., 2011, 133: 8444
29 Yang, Z., Clough, A., Lam, C.H. and Tsui, O.K.C., Macromolecules, 2011, 44: 8294
30 DeMaggio, G.B., Frieze, W.E., Gidley, D.W., Zhu, M., Hristov, H.A. and Yee, A.F., Phys. Rev. Lett., 1997, 78: 1524
31 Torres, J.A., Nealey, P.F. and de Pablo, J.J., Phys. Rev. Lett., 2000, 85: 3221
32 Fujii, Y., Yang, Z., Leach, J., Atarashi, H., Tanaka, K. and Tsui, O.K.C., Macromolecules, 2009, 42: 7418
33 Koga, T., Jiang, N., Gin, P., Endoh, M.K., Narayanan, S., Lurio, L.B. and Sinha, S.K., Phys. Rev. Lett., 2011, 107: 225901
34 Wang, Y.J. and Tsui, O.K.C., Langmuir, 2006, 22: 1959
35 Peng, D., Yang, Z. and Tsui, O.K.C., Macromolecules, 2011, 44: 7460
36 Tsui, O.K.C., Wang, Y.J., Lee, F.K., Lam, C.H. and Yang, Z., Macromolecules, 2008, 41: 1465
37 Yang, Z., Lam, C.H., DiMasi, E., Bouet, N., Jordan-Sweet, J. and Tsui, O.K.C., Appl. Phys. Lett., 2009, 94: 251906
38 Lam, C.H., Tsui, O.K.C. and Peng, D., Langmuir, 2012, 28: 10217
39 Zhao, H., Wang, Y.J. and Tsui, O.K.C., Langmuir, 2005, 21: 5817
40 Brandrup, J. and Immergut, E.H., "Polymer Handbook", 3rd ed., Wiley, New York, 1989
41 Berry, G.C. and Fox, T.G., Adv. Polym. Sci., 1968, 5: 261
42 Majeste, J.C., Montfort, J.P., Allal, A. and Marin, G., Rheol. Acta, 1998, 37: 486